Journal of Applied Fluid Mechanics, Vol. 12, No. 6, pp. 1847-1854, 2019.
Available online at www.jafmonline.net, ISSN 1735-3572, EISSN 1735-3645.
DOI: 10.29252/jafm.12.06.29581

Increase in Tuning Ability of a Car Shock Absorber Valve using CFD

D. Buczkowski† and G. Nowak

Institute of Power Engineering and Turbomachinery, Silesian University of Technology, Gliwice 44-100, Poland

†*Corresponding Author Email: daniel.buczkowski@polsl.pl*

(Received August 28, 2018; accepted February 6, 2019)

ABSTRACT

The purpose of the investigation was to improve the hydraulic damper valve to meet the automotive customer requirements. The original design was not good enough to achieve the damping forces in the range demanded. The main goal was to lower the minimum achievable forces at the compression stroke by reducing flow restrictions of piston valve. CFD analysis was used to verify proposed variants without the expense of prototyping and experimental testing. Design restrictions of present components were measured on the flow test bench and compared with previously done CFD analysis to ensure a proper correlation with a numerical model. The model was used to predict pressure drop over developed designs.

Keywords: Shock absorber; CFD analysis; Damping forces; Oil flow; Damper valve; Flow restriction.

1. INTRODUCTION

The shock absorber is responsible for safety and driving comfort of a car. The fundamental element of its operation is a valve system, that generates specific damping force characteristics, whose parameters depend strictly on the design under consideration.

In terms of conventional shock absorbers, equipped with passive damping valves, two types of them can be recognized, the mono and double-tube shock absorbers. This paper focuses on solving a problem occurring in a double-tube shock absorber, in which two valves are used; the piston valve on the rod and the base valve at the damper tube bottom. Detailed differences in design and working principles are described widely by Jamaluddin (2012), where authors provide the advantages and disadvantages of both designs and performance in handling and driving comfort.

The hydraulic damper valve systems always work in two directions, the direction of rebound and compression. These are identical with the spring and unsprung weight movement. Therefore, both directions distinguish completely different requirements for damping forces. The reason for this is the presence of the forces in the spring (compression/expansion) and the weight of the wheel (Gilles (2005). Also, a part of the energy is absorbed and released by resilient suspension components (mounting kits, rubber bumpers).

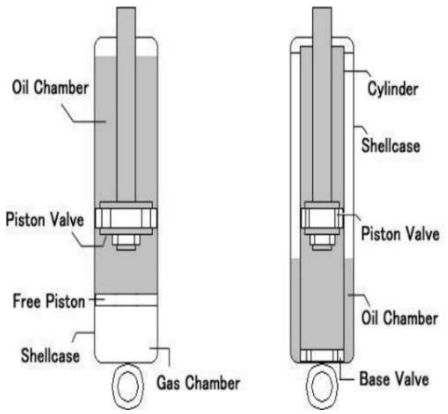

Fig. 1. Conventional shock absorber types: mono-tube/double-tube damper.

The analyzed, passive valve located on the damper piston has a relatively simple structure and consists of a piston and two sets of valve discs (metal plates) covering the appropriate holes in the piston channels. From the top and bottom, the valve is covered with washers and fixed with a nut on threaded piston post as illustrated in Figure 2 (assembled valve) and Figure 3 (exploded view). The torque is precisely specified because it influences the initial preload applied to the discs. Shaping the damping force characteristics takes place by choosing the number, diameter, and thickness of the disks on both sides of the valve. The discs deform under pressure and

create a highly restricted flow path (high oil viscosity) which results in the generation of damping forces by converting kinetic energy into heat through friction inside the fluid and the valve. Such a working principle leads to the additional challenge of providing proper heat dissipation. Otherwise, oil temperature may affect shock absorber performance (Rana *et al.* 2014).

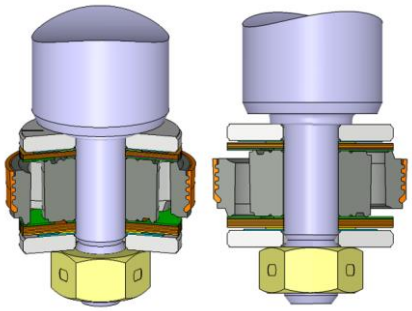

Fig. 2. View of considered piston valve.

Considered type of valve may be used in both, single and double-tube shock absorbers. The only difference is the proper selection of damping forces. During the compression stroke in a double-tube absorber, the damping forces acting on the piston valve are very small due to the presence of a base valve (bottom valve) that is in charge of generating them. Someone may wonder why there is a need to build any damping forces on the piston valve if there is another valve responsible for that. The main reason is that forces partially generated on the piston valve provide faster responsiveness of the whole system than only on the base valve.

Development of shock absorbers and its valve system requires a good understanding of physics related to working principles, conditions and developing tools to predict failures and damper performance best. For this reason, numerical analyzes are widely used in the automotive industry. They allow to reduce the costs of research and development and get detailed knowledge about the difficult to measure physical phenomena. Numerical fluid dynamics in shock absorber development serves many purposes such as determining damping characteristics, aeration conditions, pressure loads on the valve components and others. Shams *et al.* (2007) successfully used numerical analyzes to estimate the characteristics of the valve, the oil temperature influence on performance and the lift of the valve disc at a certain piston rod speed. For this purpose, they performed two independent analyses; the fluid flow one that takes into account the magnitude of valve disk deflection and the structural with pressure loads on the disk. The results of both analyses were combined to provide full knowledge about the deformation of valve discs at given operating conditions. The method used by the authors may contain inaccuracy due to uneven distribution of pressure on the disk surface which is not taken into account during the structural analysis.

Another example is an investigation of the presence of aeration using numerical methods by Czop *et al.* (2016). Their approach allowed them to develop an optimal valve shape that would withstand the increased number of load cycles without damage due to aeration effects. As can be seen, numerical calculations have become an inherent element of the research and development process of components in the automotive industry. Their possibilities will grow with the increase in computing power and the still improved solver's algorithms.

2. PROBLEM DESCRIPTION

As described in chapter 1, rebound and compression valves on piston have an independent composition of the disks on each side. However, these valves must share the single piston. Hence its shape influences the damping forces of both valves. As shown in Figure 4, a general characteristic of the valve's damping forces can be presented as the sum of curves generated by the set of disks (green line) and the High-Speed Tunning (HST) curve. The latter one has a visible effect at high velocities up to 3-4 m/s (red line).

The above information shows that the shape of the curves generated by the disk stack can be shaped in a wide range by an appropriate composition and combination of disks. However, influencing the HST curve is difficult at the tuning stage. Its shape is the result of constant flow restrictions. In some valve designs, it is possible to make it more steep by reducing the effective flow field with special covering discs. In the considered double-tube valve, solely the piston channels influenced the steepness. The main purpose was to lower down the minimum damping forces generated by HST to extend the range of available tuning. The goal was to lower the current pressure drop characteristics by at least 60%. For this purpose, a new piston design needs to be developed which has a less restrictive flow path during the compression stroke. To avoid costs associated with prototyping and testing every design version CFD analysis was applied.

Another issue requiring a reduction in piston valve flow resistance at compression is the maintenance of an appropriate pressure balance between the reflection and compression chambers. The boundary determining the balancing condition is the pressure drop across the valve towards compression, which would result in the vacuuming of the upper chamber with the risk of aeration (Czop *et al.* 2016). Oil aeration phenomena are associated with a significant, uncontrolled, but temporary drop in damping forces, so it is highly undesired.

3. MEASUREMENTS

3.1. Test Bench Description

To validate the numerical models used a flow test bench was built. It allows measuring the flow restrictions through the shock absorber valve. The measurement method guaranteed to obtain pressure values generated by the valve without the influence of other factors that could disturb the comparison

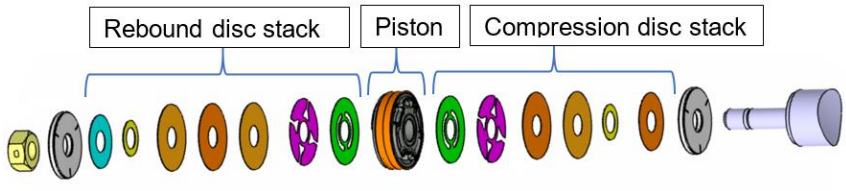

Fig. 3. Exploded view of valve composition.

such as damper pipe deformation, rod sealing friction, the gas fill pressure difference between dampers. Such measurements would be desirable to determine the quality and reproducibility of the production process (Konieczny *et al.* 2013), however, for this work it was necessary to compare isolated valves to reduce the spread of the results.

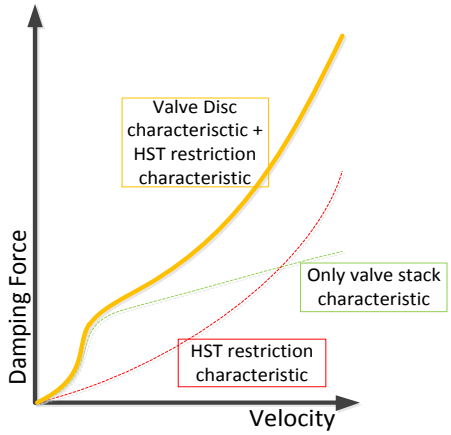

Fig. 4. Formation of damping force characteristics.

The test bench consisted of a metal column corresponding to the inner diameter of the damper tube in which the valve was placed. It has been initially fastened to a specially prepared section of the rod with shortened length to fit in the chamber. That assembly was closed inside the column with a sealed nut as presented in Fig. 5b. Two channels were led to the column, above and below the valve, through which the oil was pumped. The stand was equipped with a three-way valve that allows the direction of flow to be controlled easily. In the hydraulic system of the station, the same oil is used as in actual shock absorbers. The flow is provided with two pumps working in series. The pressure drop measurement on the tested valve took place on the inflow and outflow channel. After the valve measurements, an additional measurement of the flow resistance of the test bench itself (without the presence of a valve in a metal column) was done. It must be taken into account and subtracted from the measurement results, to achieve real pressure drop values.

3.2. Measurement Method

In the first phase, the flow restriction measurements of the original piston version were made to obtain a correlation with the previously created CFD model. Then, after the new piston project gave satisfying pressure drop results from the numerical analysis, the prototype was made and measured on the test bench using the same method as the original.

The measurements were performed with the full set of discs on the rebound side to ensure proper direction of flow at the inlet to the piston channels and lack of discs on the compression side. The measurement was carried out in the range of the flow 0-90 l/min. For each of the piston designs (Original / Design 1), three samples were tested. For each sample, three measurements were made. No differences in results between repetitions using the same sample were observed. Pressure drop results over 6 samples of measured designs are presented in Fig. 6.

The maximum uncertainty of measurement using Eq. (1) was determined as 0.05 bar and standard deviation 0.15bar.

$$s_{\bar{x}} = \sqrt{\frac{1}{n.(n-1)}.\sum_{i=1}^{n}(\bar{x}-x_i)^2} \qquad (1)$$

where:

n - amount measurements

$\bar{x}$ – aritmetic mean value

x_i – a single measurment result

Results differences between samples may come from manufacturing tolerances of pistons.

4. NUMERICAL MODEL

4.1. Geometry and Model Discretization

The solid models of the selected piston designs were prepared with CATIA V5 software. The piston was covered with a single disc to provide flow restriction at the inlet to the channel corresponding to the valve discs presence at working conditions (Fig.7). Fluid (oil) domain was created over such prepared geometry.

The initial conceptual stages contained piston geometric changes limited to inlet edge smoothing; further changes also included the slot widening. The first version with compression slots widened by 38% was not influencing the rebound slots area. The second design increased compression slots area by 100%, and in consequence, it required rebound slot decreasing (Fig. 8).

The requirements related to the manufacturing process determined the considered piston designs.

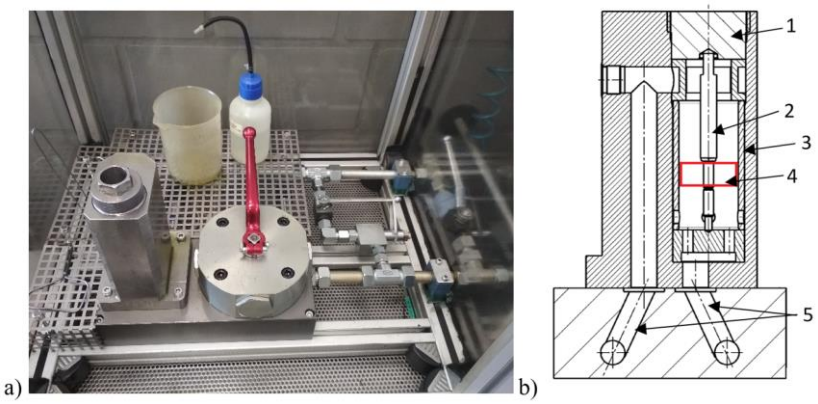

Fig. 5. a) Flow bench, b) Cross section of the metal column: 1 - Sealed nut, 2 – Pin (shortened rod), 3 – Metal sleeve (damper tube diameter), 4 - Piston valve location, 5 – Inflow/Outflow channels.

Components such as pistons are made of sintered powder metal using moulds. To reduce the cost of new parts it is recommended to use an available mould or modify the current one. Considered designs (design1/design2) are suggested by component supplier as designs demanding low-cost changes in the tooling. This limitation results in considering only individual versions, excluding the possibility of automatic design optimization.

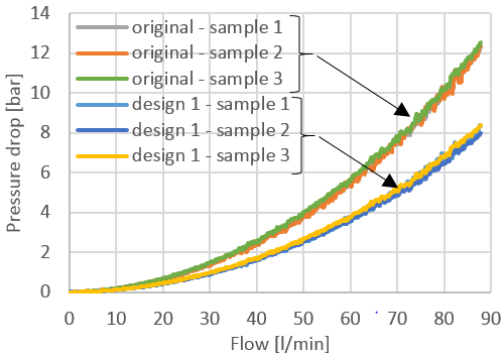

Fig. 6. Measurement results of pressure drop over original and design 1.

In addition, using the automatic optimization of the parameterized model would be very time consuming due to the complex design and changes affecting a significant number of surfaces

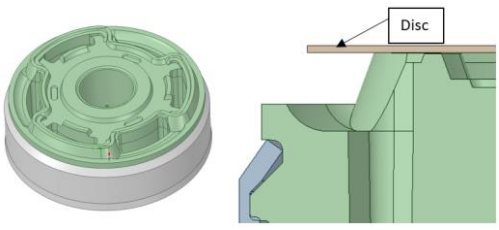

Fig. 7. Original piston design; main restriction area under disc edge at the channel inlet.

To ensure that the solution was independent of the mesh size, 4 different element sizes were investigated. It allowed recognizing the optimal amount of elements needed to provide proper accuracy without an increase in computational time. As a critical parameter of comparison, the pressure generated by the valve at flow 50l/min was used. The y^+ parameter for 600k elements mesh was ~30 to maintain elements growth rate at an acceptable level, for other it was kept at ~1.0. Results of that study are presented in Figure 9.

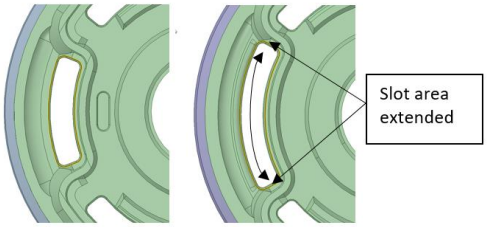

Fig. 8. Compression slot widening method.

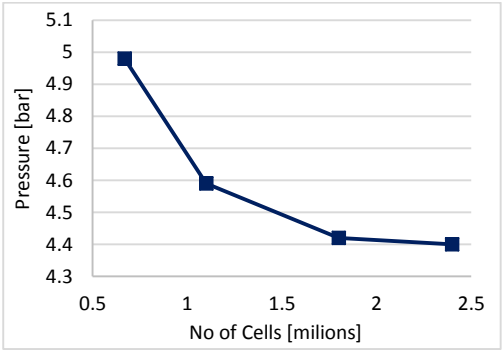

Fig. 9. Mesh independence study using original design model geometry.

Based on the results a mesh with about 1,800,000 tetrahedral cells was chosen for the flow modeling in the valve. Further, an increase in the number of cells effect in less than 1.0% difference in observed parameter and significantly extend computation time.

Figure 10 shows the details of the computational mesh for the valve model. A fine mesh was used in the regions with high-pressure gradients expected. Inflation layer elements height was set to ensure *y+* parameter value as ~1.0 at the channel inlet region, but the value varies over throughout the model up to

15.0. Such values are found to be appropriate (Guzzomi *et al.* 2007) for the turbulence modeling method and near-wall treatment approach.

In this analysis, the symmetrical half of the model was considered to limit the number of discrete elements and shorten the computational time.

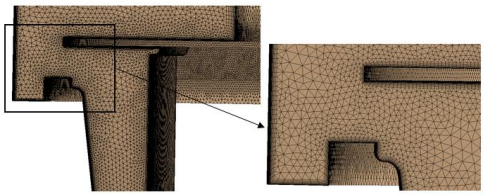

Fig. 10. CFD mesh over piston channels.

4.2. Boundary Conditions

Ansys Fluent v19.0 was selected for CFD modeling. Steady state model was prepared due to lack of moving components at considered flow conditions. Valve disc present on rebound piston side was assumed as a rigid body just like the piston geometry. At considered flow direction disc is closed and pressed to piston lands by pressure. To reduce possible edge of the disc deflection influence on flow restriction, the thickest disc from the range was used in the experiment. Actual valve with disc stacks would require an FSI analysis which would make it much more complex and time-consuming (Guzzomi *et al.* 2007).

The CFD analysis includes a numerical solution of the conservation equations in the turbulent and laminar flow regions. In this work, the finite volume method with unstructured mesh was used to solve the three dimensional incompressible Navier-Stokes equations. Pressure coupling used the SIMPLE algorithm.

The domain in which the flow was analysed was oil with parameters provided by the oil supplier; density 840 kg/m^3, dynamic viscosity 0.015 kg/m·s in 25 °C. This incompressible, viscous Newtonian fluid is assumed to have temperature-independent density and viscosity, so the model is assumed to be isothermal consistent with Guzzomi *et al.* 2007 and Kim *et al.* 2004.

The flow inlet was taken at the cross-section of the volume of fluid above the inlet to the piston channels, while the outlet was located on the other side at a distance of 30mm from the outlet of the channels to ensure proper shape of the outflow profile. A mass flow boundary condition was set at the inlet up to 0.5948 kg/s (86 l/min). The value of 86 l/min was the maximum recognized, achieved during the tests.

4.3. Turbulence Model

Because the flow in the shock absorber is turbulent, it is important to use an appropriate turbulence model to achieve reliable flow field.

Realizable k–ε model with Enhanced Wall-Treatment method was chosen to model the turbulence because it provides well-correlated results with measurements and satisfying computational time. The decision was based on unpublished results from a previously done comparison of available models with a different design than the considered one. Nevertheless, it was also focused on recognizing flow restriction generated by piston using the same oil and flow parameters. Five of the available turbulence models in Ansys Fluent software were investigated. Achieved results were compared to measurements. Relative error obtained with those models was based on maximum pressure generated by design restriction relative to the pressure achieved from measurements. For each model at every considered flow value (0-90 l/min), it was calculated as:

$$\left|\delta_j\right| = \frac{\left|p_{ij} - p_{meas.j}\right|}{\left|p_{meas.j}\right|} \tag{2}$$

where;

p_{ij} – maximum pressure generated by restriction for i-turbulence model used at j l/min flow

$p_{meas.j}$ – maximum pressure measured on the test bench at the j l/min flow

Calculated relative error values have been averaged over the flow range studied for comparison reasons (Fig. 11). Percentage value from the graph should be understood as a pressure difference between the measurement and CFD flow characteristic.

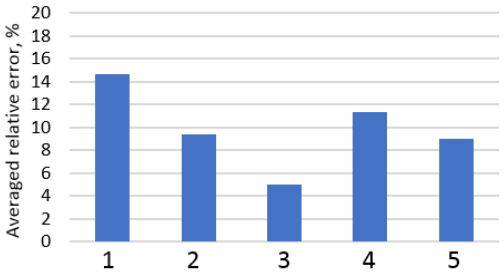

1- Standard k-epsilon (Stadard Wall Function)
2- Realizable k-epsilon (Standard Wall Function)
3- Realizable k-epsilon (Echanced Wall Function)
4- Standard k-omega
5- SST Transition

Fig. 11. The relative error of analysis using different models of turbulence relative to test results.

The popular, standard k–ε model is a semi-empirical model based on transport equations for the turbulent kinetic energy (k) and its dissipation rate (ε). While it is widely used, it still indicates a few drawbacks. Advancements have been made to the model to improve its performance by the realizable model. The realizable k–ε model is a relatively recent development and differs from the standard one in two imnportant ways. Firstly, the realizable k–ε model contains a new formulation for the turbulent viscosity. Also, a new transport equation for the dissipation rate, k–ε has been derived from the exact

equation for the transport of the mean-square vorticity fluctuation.

Transport equations for k and ε in the realizable k–ε model are:

$$\frac{\partial}{\partial t}(\rho k)+\frac{\partial}{\partial x_j}(\rho k u_j)= \frac{\partial}{\partial x_j}\left[\left(\mu+\frac{u_t}{\sigma_k}\right)\frac{\partial k}{\partial x_j}\right]+G_k+G_b-\rho\varepsilon-Y_m+S_k \tag{3}$$

and

$$\frac{\partial}{\partial t}(\rho\varepsilon)+\frac{\partial}{\partial x_j}(\rho\varepsilon u_j)= \frac{\partial}{\partial x_j}\left[\left(\mu+\frac{u_t}{\sigma_\varepsilon}\right)\frac{\partial \varepsilon}{\partial x_j}\right]+\rho C_1 S\varepsilon - \rho C_2\frac{\varepsilon^2}{k+\sqrt{\nu\varepsilon}}+C_{1\varepsilon}\frac{\varepsilon}{k}C_{3\varepsilon}G_b+S_\varepsilon \tag{4}$$

where

$$C_1=max\left[0.43,\frac{\eta}{\eta+5}\right],\eta=S\frac{k}{\varepsilon},S=\sqrt{2S_{ij}S_{ij}}$$

In those equations, G_b is the generation of turbulence kinetic energy due to buoyancy, G_k represents the generation of turbulence kinetic energy due to the mean velocity gradients, Y_m is the contribution of the fluctuating dilatation in compressible turbulence to the overall dissipation rate, C_2 and $C_{1\varepsilon}$ are constants, σ_k and σ_ε are turbulent Prandtl numbers for k and ε, respectively. S_k and S_ε are user-defined source terms.

The k Eq. (3) is the same as that in the standard k–ε model, except for the model constants. However, the form of the ε equation is quite different from those in the standard k–ε models. One of the noteworthy features is that the production term in the ε equation (the second term on the right-hand side of Eq. (4)) does not involve the production of k. It is believed that this form is better in representing the spectral energy transfer. Another desirable feature is that the destruction term (the third term on the right-hand side of Eq. (4)) does not have any singularity; that is, its denominator never vanishes, even if k vanishes or becomes smaller than zero. This feature is contrasted with traditional k–ε models, which have a singularity due to k in the denominator.

This model has been thoroughly validated for a wide range of flows (Kim *et al.* 1997; Shih *et al.* 1995) including channel flows and boundary layers, rotating homogeneous shear flows, free flows including streams and mixing layers, and separate flows. In these cases, it was found that the performance of the model is much better than the standard k-ε (ANSYS User's Guide 2013).

5. RESULTS AND DISCUSSION

The results of the CFD analyzes of all considered designs compared at maximum flow are presented in Figure 12. The required level of design restriction is marked with the red line.

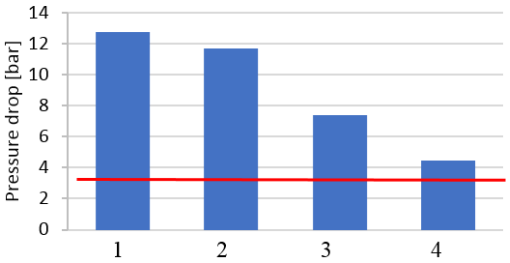

Original design
1- Original design (smothed inlet)
2- Desgin 1
3- Desgin 2

Fig. 12. Pressure drop at 86 l/min - CFD results.

In the graph, we can notice that the influence of changes limited to the smoothing of the inlet edge to the channel resulted in a slight pressure drop, and the obtained result was far from expected (red line). Design 2 was the first which generates less than the required pressure drop at the maximum flow rate of 86 l/min. Below the results of the original and two promising piston designs with extended piston slots are presented (Fig. 13), combined with the results of measurements.

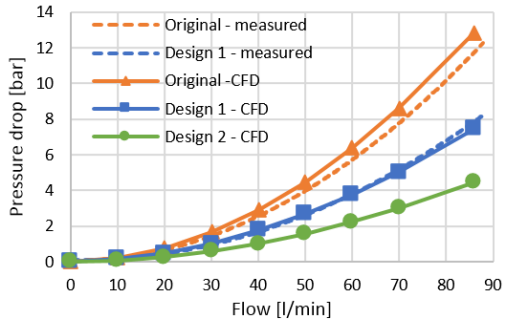

Fig. 13. Pressure drop results.

If we compare the results, a satisfactory correlation can be found with the experimental data, where the maximum discrepancy did not exceed 10% (original design). A similar level of accuracy was obtained by researchers using very close numerical model settings but a different way of measuring the damping forces (Shams *et al.* 2007). Difference between correlation for original and wider slot design (Design 1) may be the effect of the better adjustment of the $y+$ parameter within the channel due to lower velocity gradients and fewer vortexes due to the smoother flow path. Design 1 reduced the pressure generated by the restriction by 45% and the second project (Design 2) by almost 75% reaching the assumed level of flow resistance. Design 2 can be successfully used to reach customer damping force requirements at compression.

Below are presented both pressure and velocity distributions in the symmetrical plane of the cross-section of the piston channel covered by the disk.

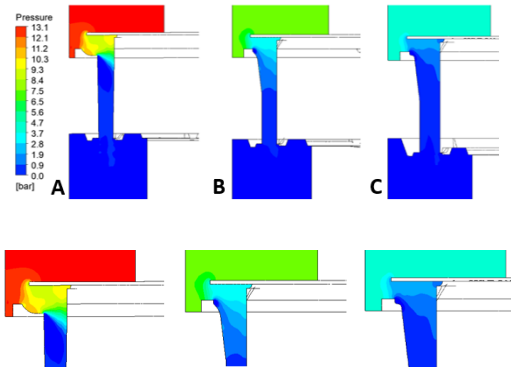

Fig. 14. Pressure distribution over considered designs at symmetry plane through the channel, A- Original, B- Design 1, C- Design 2.

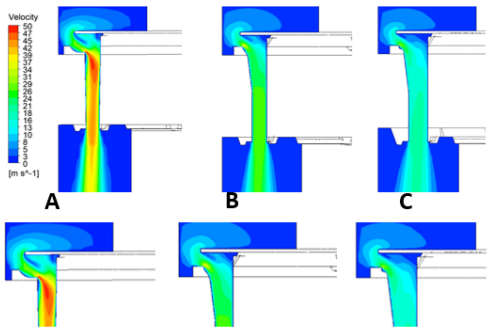

Fig. 15. Velocity distribution over considered designs at symmetry plane through the channel, A- Original, B- Design 1, C- Design 2.

Implemented design modifications lead to move the main pressure drop region from deep channel inlet into the valve disc edge (Fig. 14). Despite this, the top/bottom average pressure difference over unsupported disc region is almost the same.

It can be noticed that there is no separation of the accelerated stream after removing the sharp edge at the inlet of the channel and velocity profile is more homogeneous. The pressure scale has been cut at 0 bar to improve the visibility of the results (Fig. 14, Fig. 15).

6. CONCLUSIONS

The effect of the analysis presented in this work was to determine the design of the piston, which meets the initially assumed requirements. The costs related to the implementation of intermediate versions and their testing were reduced by using CFD models, which determined the restrictions of the considered designs. The piston version with the largest effective flow area, allowed to reduce the generated pressure by 75% relative to the original construction which will significantly affect the range of small forces, possible to be obtained by the considered valve. Due to the design impact on rebound channels flow area, it will be necessary to examine their restrictions, which may significantly increase. Usually demanded high damping forces at rebound will cause that higher restrictions in this direction which can be easily compensated by the appropriate composition of the valve disks.

Valve disc behaviour as rigid body was assumed during CFD simulations what may lead to worse correlation. A significant widening of the channel inlet results in a reduction of the disc outer edge support region (piston lands). Therefore, it may cause excessive deflection of the disk edge to the inlet of the channel due to the pressure difference above and below the disc in this region. That will effect in higher flow restriction because of closing flow path by the edge of the disc. Possible influence of that can be seen on Figure 13 as differences between measurement-CFD correlations of original piston and design 1. The plastic deformation of the disk due to this load can have an uncontrollable effect on the damping characteristics and fatigue strength of the entire set of disks. The next step should be the structural analysis of the discs based on the new design of the piston loaded with pressure occurring under standard operating conditions.

7. ACKNOWLEDGMENTS

This research was co-financed by the program of Ministry of Science and Higher Education, PhD thesis implementation in industry, contract number 11/DW/2017/01/1. Additionally, authors are grateful to Tenneco company for good cooperation and the opportunity to publish research results.

8. REFERENCES

ANSYS Fluent User's Guide (2013), ANSYS, Inc., Southpointe, 275 Technology Drive, Canonsburg, PA 15317, Release 15.0.

Czop, P. and J. Gniłka (2016). Reducing aeration and cavitation effect in shock absorbers using Fluid-structure interaction simulation. *Computer Assisted Methods in Engineering and Science* 23, 171–189.

Gilles, T. (2005). *Automotive Chassis: Brake*, Steering & Suspension,

Guzzomi, F. G., P. L. O'Neill and A. C. R. Tavner (2007). *Investigation of Damper Valve Dynamics Using Parametric Numerical Methods*, School of Mechanical Engineering, University of Western Australia, 6009 AUSTRALIA.

Jamaluddin, M. S. (2012). *A Study of The Causes Of Bouncing Problems Of Shock Absorber*, Faculty of Manufacturing Engineering, Universiti Malaysia Pahang.

Kim, C., C. Y. Perng and D. Zhang (2004). Transmission Main Control Orifice Flow Characteristics and Correlations. *SAE technical paper* No. 2004-01-1639, Society of Automotive Engineers.

Kim, S. E., D. Choudhury and B. Patel (1997). Computations of Complex Turbulent Flows Using the `Commercial Code ANSYS Fluent. *In Proceedings of the ICASE/LaRC/AFOSR*

Symposium on Modeling Complex Turbulent Flows. Hampton, Virginia.

Konieczny, L., R. Burdzik and J. Warczek (2013). The Uncertainty of Determining Shock Absorber Damping Characteristic on Indicator Test Stand, *Diagnostyka* 14(2), 63-66.

Rana J., S. Gajjar and A. Patel (2014). Experimental Analysis and Heat Transfer Study of Damping Fluid in Shock Absorber Operation. *IJEDR* 2(3), 2939-2947.

Shams, M., R. Ebrahimi, A. Raoufi and B. J. Jafari (2007, October). CFD-FEA Analysis Of Hydraulic Shock Absorber Valve Behavior. International *Journal of Automotive Technology* 8(5), 615-622.

Shih, T. H., W. W. Liou, A. Shabbir, Z. Yang and J. Zhu (1995). A New k- ε Eddy-Viscosity Model for High Reynolds Number Turbulent Flows - Model Development and Validation. *Computers Fluids* 24(3), 227–238.